ELSEVIER

Journal of Nuclear Materials 265 (1999) 28–37

journal of nuclear materials

Effect of Mo on recrystallization characteristics of Zr–Nb–(Sn)–Mo experimental alloys

Y.B. Chun [a], S.K. Hwang [a,b,*], M.H. Kim [a], S.I. Kwun [c], Y.S. Kim [d]

[a] *Department of Metallurgical Engineering, Inha University, 253 Yonghyun-Dong, Nam-Gu, Inchon, 402-751, South Korea*
[b] *Jointly Appointed at the Center for the Advanced Aerospace Materials, South Korea*
[c] *Department of Materials Science and Engineering, Korea University, Seoul, 136-701, South Korea*
[d] *Korea Atomic Energy Research Institute, Daejeon, 305-353, South Korea*

Received 11 August 1997; accepted 7 October 1998

Abstract

Feasibility of using Mo as a crucial alloying element in Zr-based alloys is addressed in terms of grain growth characteristics, texture and mechanical properties. In binary Zr–1Nb alloy, addition of Mo retarded recovery and recrystallization of cold worked microstructure and suppressed grain coarsening. Mo also prevented abnormal grain growth that occurred in the binary alloy. The grain refinement effect of Mo was explained in terms of β-phase forming at the interface of α-phase plates. Yield strength and ultimate tensile strength of heat-treated Zr–1Nb and Zr–1Nb–ySn-0.1Fe alloys were also enhanced by Mo addition due to solid-solution hardening and persistent cold-worked dislocation substructure. As cold-rolled Zr–1Nb alloys showed a rather high basal texture along the normal direction of plate surface and this was relaxed by Mo addition, which was attributed to grain refinement and promotion of β-phase. The present work indicates that Mo can be a valuable addition in Zr-based alloys particularly under extended high temperature exposure.

PACS: 81.05.BX

1. Introduction

In accordance to the high burn-up requirement in water reactors [1,2] demands arise for better core materials based on Zr. High strength as well as high creep resistance are sought in addition to the corrosion resistance for fuel cladding or pressure tube applications. For this purpose, the target chemical constituents of advanced zirconium alloys have been centered around Zr–Nb and Zr–Nb–Sn with possible addition of Mo. Many alloys have been already developed based on Zr–Nb–Sn system: for example, ZIRLO [3] and E635 [4]. In case of EXCEL [5], a noticeable amount of Mo was added to enhance creep resistance and solid solution hardening. Although the usage of Mo as a major alloying element in advanced zirconium alloys has been so far rather limited particularly because of a concern on formability, it deserves more attention when creep situation is seriously considered.

The role of Mo in zirconium alloys is not fully understood. According to Williams et al. [6] and Carpenter et al. [7] Mo promotes solid solution hardening and precipitation hardening in Zr–Nb–Sn or Zr–Al alloys. In addition, Hwang et al. [8] reported a grain-refining effect and a texture-relieving effect of Mo. As a β-stabilizer, Mo also affects phase transformation of Zr. In the present work, we attempted to answer the questions on how and why Mo-containing zirconium alloys resist grain growth and also, on whether Mo addition is to be favorably considered in the future alloy development.

2. Experimental procedure

Plasma arc melting with water-chilled copper hearth was used to prepare experimental alloys. Basically two

* Corresponding author. Tel.: +82-32 860 7537; fax: +82-32 862 5546; e-mail: skhwang@inha.ac.kr.

0022-3115/99/$ – see front matter
PII: S0022-3115(98)00651-5

groups of experimental alloy compositions were prepared: Zr–1Nb–xMo group to study the basic effect of Mo on grain growth characteristics and Zr–1Nb–ySn–xMo–0.1Fe group to evaluate the mechanical properties. Nuclear grade sponge Zr and Nb and Mo 99.9% and 99.95% in purity, respectively, were used for melting. The alloys of the chemical compositions as shown in Table 1 were made into buttons of 300 g in weight, and were forged at 1100°C to reduce the thickness by 60%. Hot rolling was conducted at 800°C to give 50% reduction in thickness. Prior to hot rolling buttons were enwrapped with stainless steel sheets and soaked at 1000°C for 20 min, followed by water quenching. Final deformation was conducted at room temperature by cold rolling the hot-rolled plates into thin plates of 3 mm in thickness, which was equivalent to a reduction of 25%. For Zr–1Nb–ySn–xMo–0.1Fe alloys, additional β heat treatment of 1000°C for 10 min and air cooling was conducted prior to the final cold rolling.

For texture analysis, Kearns numbers of experimental alloy plates were measured by X-ray diffraction method according to the procedure described elsewhere [9]. Relative amount of β-phase in the α-matrix was measured also by the X-ray diffraction method as suggested by Gazzara [10]. Tensile testing was conducted at room temperature and also at 385°C. Flat tensile test specimens (ASTM E8 sub-size, 10 mm in gage length) were cut from the cold rolled plates such that the tensile loading axis was parallel to the rolling direction. A crosshead speed of 2 mm/min was maintained during testing. Etching solution for optical microscopy and electropolishing solution for TEM were composed of $HF:HNO_3:H_2O = 5:45:50$ in volume and $HClO_4:CH_3OH = 1:4$ in volume, respectively.

3. Results and discussion

3.1. Grain refining effect of Mo

An optical micrograph of experimental Zr–1Nb alloy in the as cold-rolled condition is shown in Fig. 1. Grains consisted of basket-weave type elongated plates, the details of which were not clearly resolved because of the low magnification. As for the effect of Mo, there was no clear difference in the optical micrographs of as cold-rolled samples regardless of Mo content. The microstructural features in the as cold-rolled condition were similar to those of commercial Zr–2.5Nb alloy [11] and of Zr–Nb–Sn alloy (ZIRLO).

TEM micrographs of as cold-rolled samples of Zr–1Nb and Zr–1Nb–0.7Mo alloys are shown in Fig. 2. In both samples, a high density of dislocations was observed. A significant difference in the two alloys was in the distribution of the second phase β. The β-phase in both alloy systems existed predominantly along the boundaries of α-laths as a platelet shape. However, the morphology of β-phase was different in that the phase was more continuous in Zr–1Nb–0.7Mo alloy. Despite the morphological difference detectable by TEM, it was not as great as to be discernible by XRD analysis in the as cold-rolled condition. Only after extended recrystallization annealing treatment, variation in the amount of β-phase became substantial: 2% vs. 11% for Zr–1Nb and Zr–1Nb–0.7Mo alloys, respectively, after 16 days of annealing at 700°C. Evolution of β-phase during extended heat treatment of both alloys is shown in Table 2 and Fig. 3. The amount of β-phase increased with Mo content, which was most significant for the alloys containing more than 0.3 wt% of Mo.

Table 1
Chemical compositions of experimental alloys

Nominal	Analysis (wt%)				
	Nb	Sn	Mo	Fe	Zr
Zr–1Nb	1.01	–	–	–	
Zr–1Nb–0.1Mo	1.07	–	0.11	–	
Zr–1Nb–0.3Mo	1.02	–	0.33	–	
Zr–1Nb–0.5Mo	0.94	–	0.51	–	
Zr–1Nb–0.7Mo	0.96	–	0.68	–	
Zr–1Nb–0.5Sn–0.1Fe	0.99	0.50	–	0.13	
Zr–1Nb-0.5Sn–0.2Mo–0.1Fe	0.98	0.51	0.21	0.14	
Zr–1Nb–0.5Sn–0.5Mo–0.1Fe	0.95	0.50	0.51	0.16	
Zr–1Nb–0.5Sn–0.7Mo–0.1Fe	0.92	0.50	0.71	0.15	Bal.
Zr–1Nb–0.7Sn–0.1Fe	0.95	0.66	–	0.13	
Zr–1Nb–0.7Sn–0.2Mo–0.1Fe	0.89	0.68	0.22	0.15	
Zr–1Nb–0.7Sn–0.5Mo–0.1Fe	0.98	0.70	0.53	0.15	
Zr–1Nb–0.7Sn–0.7Mo–0.1Fe	1.06	0.69	0.74	0.15	
Zr–1Nb–1Sn–0.1Fe	1.02	0.94	–	0.15	
Zr–1Nb–1Sn–0.2Mo–0.1Fe	0.97	0.92	0.19	0.14	
Zr–1Nb–1Sn–0.5Mo–0.1Fe	1.00	0.92	0.50	0.16	
Zr–1Nb–1Sn–0.7Mo–0.1Fe	1.00	0.90	0.67	0.16	

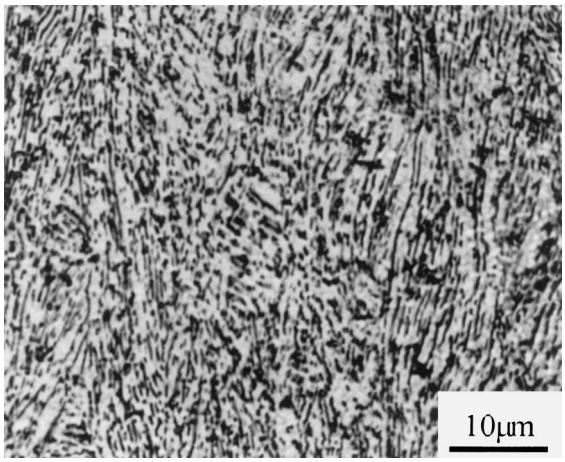

Fig. 1. Optical micrograph of as cold-rolled Zr–1Nb alloy.

Details of microstructural development of Zr–1Nb alloy during heat treatment at 700°C are shown in the TEM micrographs of Fig. 4. In this alloy recovery occurred in 1 h at the temperature, resulting in subgrains within dislocated α-laths as shown in Fig. 4(a). As the heat treating time was prolonged, the dislocation substructures in the cold-rolled samples underwent a considerable change, leading to recrystallization. Apparently the rate of recrystallization was uninfluenced by the presence of Mo. Instead, the microstructural change of α laths during recrystallization was accompanied by decomposition of β-phase at the lath boundaries. Because of the stabilizing effect of Mo, the β-phase in Zr–1Nb–*x*Mo alloys better resisted against the decomposition than that in the binary Zr–1Nb alloy did.

While the evolution characteristics of the substructure during recrystallization, except for the β-phase, were more or less the same for the all alloy compositions, a peculiar feature was observed in the Mo-free Zr–1Nb alloy during extended annealing. Abnormal grains were observed as shown in Fig. 4(b), the size of which ranged from 5 to 20 μm in diameter compared to 0.5–1 μm of normal recrystallized grains. The abnormal grain size distribution was established at about 1 h of heat treatment at 700°C and lasted up to 20 h, when normal grain growth took over. When the abnormal grains first appeared, the distribution of the grain size became bimodal. As the heat treating time was prolonged, however, small grains were coalesced into neighboring large grains. The large grains then filled the entire space and started normal grain growth. Inside the abnormal grains, resided many particles of β-phase that probably resulted from decomposition of thin β-platelets at α-lath boundaries. During recovery and recrystallization of α-laths, the continuity of the thin β-phase was broken presumably due to spheroidizing of the phase itself.

Several factors contribute in abnormal grain growth of metal alloys, the most prominent one being the presence of a restraining force against grain growth [12]. Typical origins of the restraining forces are second phase particles, free surface and crystallographic texture. In case of the second phase particles, abnormal grain growth may occur when the areas constrained by the particles, usually less than 10% in volume, and unconstrained areas are co-present [13]. This theory is applicable to the present case, considering the role of β-phase as the constraint second phase. A mere presence of β-phase, however, does not fully explain the case of abnormal grain growth. There is a complexity associated

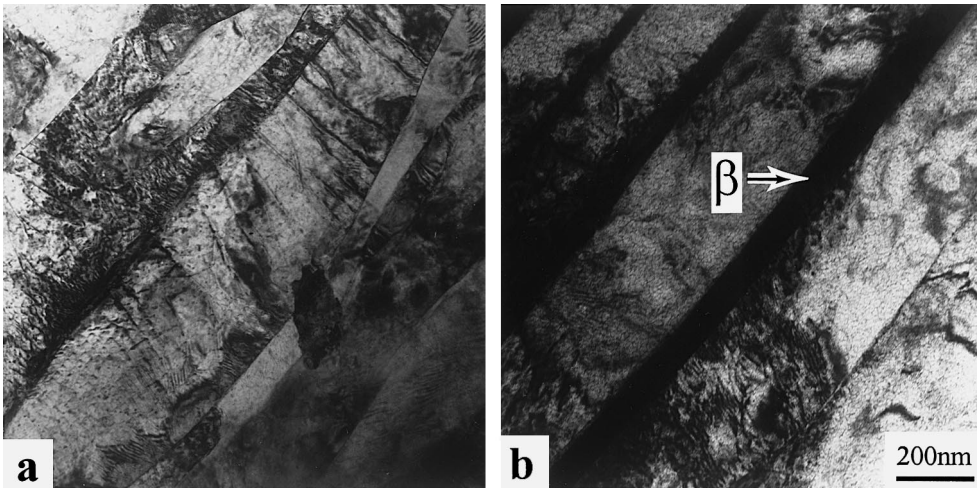

Fig. 2. TEM micrographs of as cold-rolled (a) Zr–1Nb alloy and (b) Zr–1Nb–0.7Mo alloy. While Zr–1Nb contained β-phase discontinuously scattered along the lath boundaries Zr–1Nb–0.7Mo alloy exhibited continuous β-platelets, as marked in the photograph, covering lath boundaries.

Table 2
Amount of residual β phase (in vol%) of experimental Zr–1Nb–*x*Mo alloys annealed at 700°C

Alloys	Time at 700°C		
	54 h	148 h	398 h
Zr–1Nb	1	1	2
Zr–1Nb–0.1Mo	1	3	3
Zr–1Nb–0.3Mo	1	5	3
Zr–1Nb–0.5Mo	7	7	10
Zr–1Nb–0.7Mo	6	10	11

with the transformation route and the stability of this phase, which is explained below.

Abnormal grain growth in Zr–1Nb alloy is presumably is a result of either unrestrained fast movement of α-lath boundaries or coalescence of two closely oriented α laths. The first mechanism is as follows. During hot rolling at 800°C, samples are exposed to α + β range and α-laths form at β boundaries during subsequent cooling. Due to the solubility difference α and β, Nb is expelled from the newly formed α to the lath boundaries. Since Nb is a β-stabilizer this results in thin layers of β-phase at lath boundaries. If the amount of Nb is insufficient to cover every lath boundary then some boundaries will be short of the restraining force against the curvature-driven movement toward coarsening. As a result, a few unconstrained grains grow fast during the last stage of recrystallization. Blockage of lath boundaries may also become ineffective if the β-phase at the boundaries spheroidizes.

The coalescence mechanism of abnormal grain growth in Zr–1Nb alloy is active when there are two adjacent α-laths of the same crystal orientation. During hot rolling process α-laths form from pre-existing

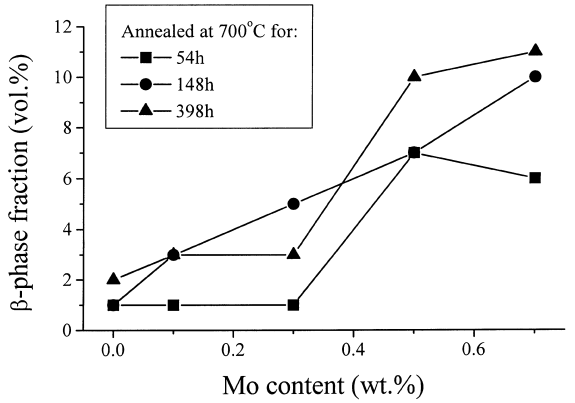

Fig. 3. Variation in the amount of β-phase of heat-treated experimental Zr–1Nb–*x*Mo alloys.

β-grains. The α-laths generally assume different crystal orientations each other. If two adjacent laths accidentally have the same crystal orientations as a result of the phase transformation then they tend to coalesce. The situation may become complex when martensitically transformed α′ phase and diffusionally transformed α phase co-exist [14].

Presence of Mo in the alloy composition efficiently suppressed the abnormal grain formation as shown in the optical micrographs of Fig. 5. All the samples for the microscopy, Zr–1Nb–*x*Mo in composition, were heat treated for 20 h at 700°C. While the samples containing up to 0.3 wt% Mo showed abnormal grain growth in some areas the samples containing higher amount of Mo showed only normal grain growth.

The role of Mo in suppressing abnormal grain growth in Zr–1Nb alloy may be attributed to two

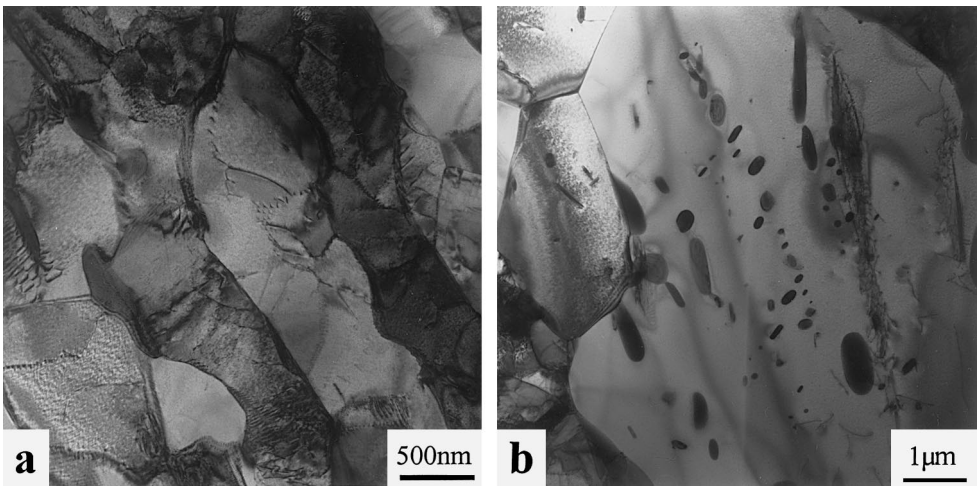

Fig. 4. TEM micrographs of Zr–1Nb alloy heat treated for 1 h at 700°C showing (a) subgrain formation in α-laths and (b) an abnormal grain, showing debris of β-phase particles inside.

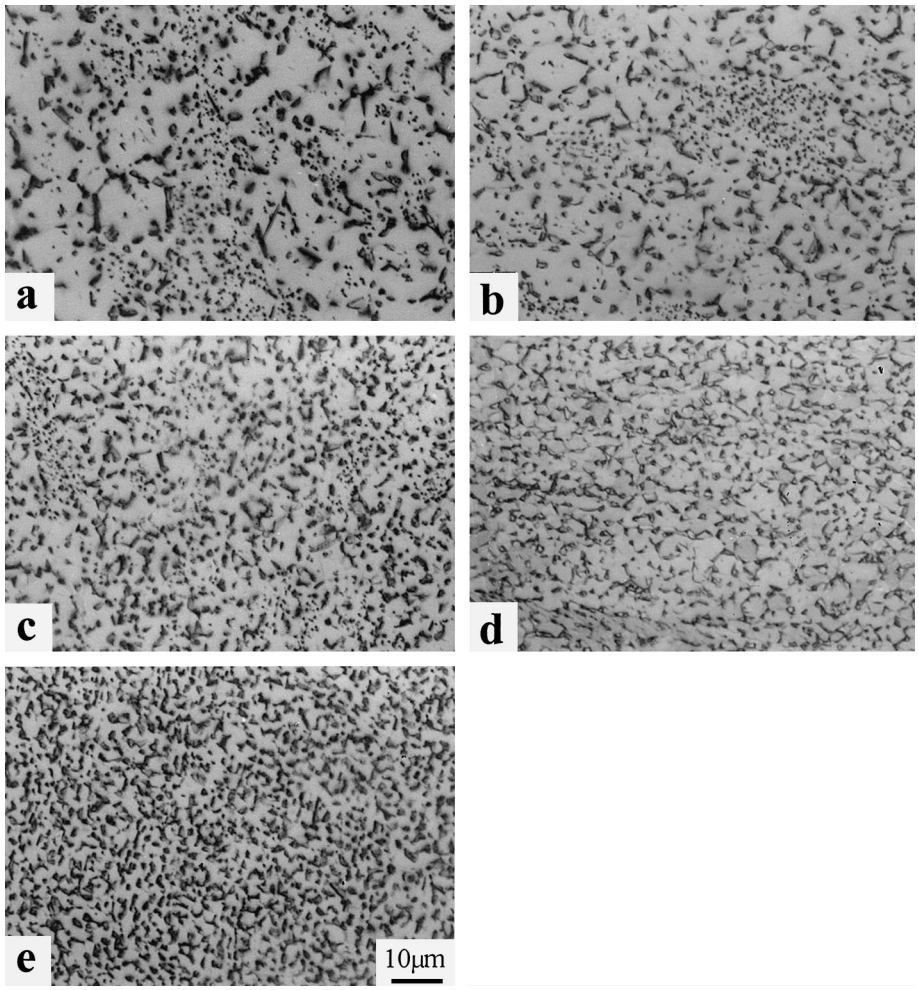

Fig. 5. Optical micrographs of (a) Zr–1Nb alloy (b) Zr–1Nb–0.1Mo alloy, (c) Zr–1Nb–0.3Mo alloy, (d) Zr–1Nb–0.5Mo alloy and (e) Zr–1Nb–0.7Mo alloy, all heat treated at 700°C for 20 h. Note the abnormal grain growth in the alloys with the lean content of Mo.

factors, stability of β-phase and solute dragging effect. Being a β-stabilizer, Mo increases the amount as well as the stability of β-phase. Like Nb, Mo is expelled from α-lath interior to the lath boundaries, promoting β formation at the lath boundaries. With the aid of Mo, therefore, β-phase becomes more stable and uniformly distributed. In this respect, there seems to be a critical amount of Mo to be effective. From the results shown in Fig. 5, the critical amount appears to be 0.5 wt%.

In addition to the suppression of abnormal grain growth, addition of Mo into Zr–1Nb also resulted in general grain refinement as shown in Table 3 and Fig. 6. The general grain refining effect of Mo may also be explained on the grounds proposed above. As shown in Table 3, Zr–1Nb–0.7Mo alloy showed no significant grain growth even after 148 h of exposure at 700°C. Moreover the effect was persistent in the single β field at higher temperature. The microstructures of Zr–1Nb and Zr–1Nb–0.7Mo alloys obtained by β-annealing at 1000°C are shown in Fig. 7, which demonstrates again the grain refining effect of Mo. In this case, however, the mechanism of grain refinement in the Mo-containing alloy is different from that at 700°C case. Since there is only the equilibrium β phase at 1000°C, a restraining force against boundary movement is not expected. Instead, it is possible that a solute-dragging effect of Mo was responsible for the retarded boundary movement. In fact, a possibility of Mo segregation on grain boundaries was raised by Heritier and Jonas [15].

3.2. Texture relaxation effect of Mo

Effect of Mo on crystallographic texture was measured by the Kearns number, the variation of which are shown in Table 4 and Fig. 8. for experimental Zr–1Nb–*x*Mo alloys and Zr–1Nb–1Sn–*x*Mo–0.1Fe alloys. The

Table 3
Grain size (mean diameter in μm) of experimental Zr–1Nb–*x*Mo alloys annealed at 700°C

Alloys	Time at 700°C		
	54 h	148 h	398 h
Zr–1Nb	9.1	10.2	16.1
Zr–1Nb–0.1Mo	7.1	8.7	12.5
Zr–1Nb–0.3Mo	5.4	6.0	9.8
Zr–1Nb–0.5Mo	4.5	5.9	9.8
Zr–1Nb–0.7Mo	4.1	4.7	6.4

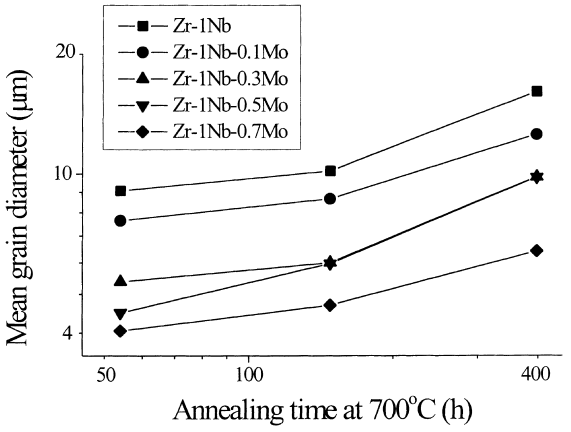

Fig. 6. Grain size variations of experimental alloy with annealing time at 700°C.

alloys without Mo showed a strong basal texture along the direction normal to the surface of plate. In both alloy systems Mo decreased the normal basal texture under all heat treatment conditions as shown in Fig. 8(a) and (b). The texture variation with the heat treatment was such that the normal texture increased and then either saturated or decreased with time at temperatures as shown in Fig. 8(c). Generally the annealing texture of Zr sheets is a function of heat treatment. Strengthening of the basal texture during recrystallization annealing heat treatment occurs in Zircaloys. For example Rogerson [16] reported that the Kearns number along the radial direction of Zircaloy-2 tube, which is equivalent to the normal direction of thin plates, increased from 0.4 in cold worked condition to 0.7 in recrystallization annealed condition. Development of the non-basal texture along the surface normal direction has been also reported by Cheadle et al. in thin plates of EXCEL alloy [17].

Crystallographic texture in Zr-based alloys develops during plastic deformation due to insufficient slip system [18,19]. In case of plate rolling, the deformation consists of compressive strains in the normal direction and large tensile strains in the rolling direction. The basal poles tend to orient toward the axis of the compressive strain. Twinning on $\{1\ 0\ \bar{1}\ 2\}$ planes is an important mechanism of deformation at room temperature particularly when the amount of deformation is small (up to about 20%) [20–22]. A consequence of twinning is to orient [0 0 0 2] basal poles toward the surface normal direction of plates. At larger degree of deformation $\langle c+a\rangle$ slips become active and re-orient the basal poles, resulting in biomodal peaks inclined along the normal-transverse direction.

Among many factors affecting the texture of Zr-based alloys, such as the chemical composition and the mode of working [23], the texture variation with Mo content in the present study seems strongly related to the grain size. The grain size effect on the texture of Zr–2.5Nb alloy was reported by Salinas-Rodriguez [24]. Large grain size induces twinning during plastic deformation whereas small grain size promotes slip, with the consequence of a strong [0 0 0 2] texture and intermediate $\langle 1\ 1\ \bar{2}\ 0\rangle$ fiber texture, respectively. In the present case, Mo-addition resulted in grain refinement as described above, which weakened the normal basal texture.

Another factor affecting the texture of the present experimental alloys is the presence of β-phase. As shown above, the amount as well as the stability of β-phase increased with the amount of Mo added. Upon cooling from high temperature, the low temperature matrix phase α inherits its texture from the high temperature β-phase according to the Burgers relationship [25]. Retention of β-phase in the α-matrix will randomize crystal orientations because α-laths maintain crystal orientation relationships with β-phase randomly located at boundaries of α-laths. Therefore it is possible to control texture by controlling phase transformation routes. For example, a strong basal texture can be obtained by a controlled step cooling heat treatment from the β-phase [14,26] in which diffusional transformation of β to α predominates over martensitic transformation.

In addition to the reasons given above, there may be yet another effect of Mo on texture through modifying the high temperature deformation mechanism. As suggested by Povolo et al. [27], the distribution of the [0 0 0 2] component varies during creep in the way that the location of the bimodal peaks of the basal component rotates from the tangential-normal direction toward the normal-rolling direction. Although it remains to be confirmed, there is a good possibility of Mo affecting the mode of deformation during hot rolling that occurs mainly by the prism slip and $\langle c+a\rangle$ slip.

Depending on applications, Zr-based alloys require different degree of the basal texture. For Zircaloy fuel cladding tube application, a high radial texture is desirable to minimize the susceptibility to iodine-induced stress corrosion cracking [26,28,29]. For pressure tube application of heavy water reactors, on the other hand, a

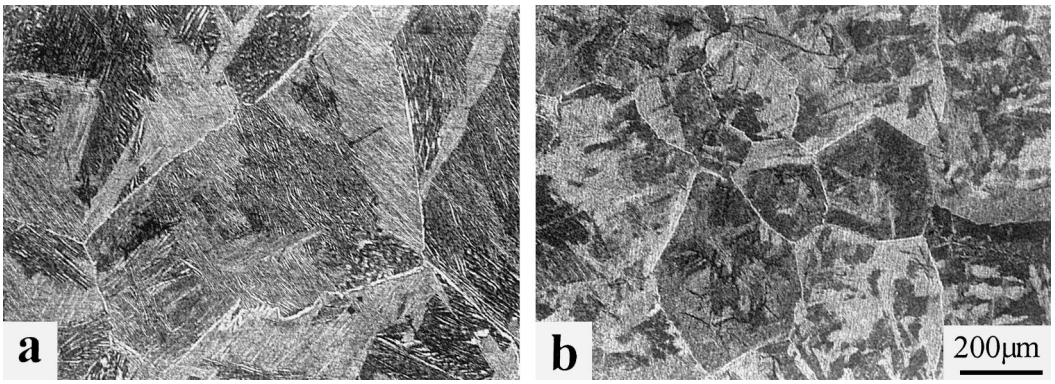

Fig. 7. Optical micrographs of (a) Zr–1Nb alloy and (b) Zr–1Nb–0.7Mo alloy, all heat treated at 1000°C for 30 min and furnace cooled.

strong transverse basal texture, such as that in Zr–2.5Nb alloy [30], is more resistant to diametrical strain induced by irradiation creep and growth [23].

3.3. Strength enhancement effect of Mo

The tensile properties of experimental Zr–Nb–*y*Sn–*x*Mo–0.1Fe alloys are presented in Table 5 and those of Zr–1Nb–1Sn–*x*Mo–0.1Fe alloys are illustrated in Fig. 9 as a function of Mo content. Addition of Mo increased the yield strength and the ultimate tensile strength regardless of the alloy system. Tensile ductility at room temperature decreased with Mo content while that at elevated temperature was less sensitive to Mo content. Solid-solution hardening effect and stabilization of dislocation substructure due to Mo are responsible for the strength enhancement in the Zr–1Nb–1Sn–*x*Mo–0.1Fe alloys.

For the purpose of strengthening, Mo addition is a valuable addition in Zr-base alloys. In case of PWR fuel cladding or HWR pressure tubes, the final process step of Zr-based alloys involves cold working that serves as shaping method as well as strengthening technique. Excessive amount of cold working, however, is detri-

Table 4
Variation of the basal texture (measured by the Kearns number) of experimental Zr–1Nb–*x*Mo alloys and Zr–1Nb–*y*Sn–*x*Mo–0.1Fe alloys

	f_n (as cold-rolled)	f_n (annealed at 700°C)		
		54 h	148 h	398 h
Zr–1Nb	0.62	0.56	0.58	0.61
Zr–1Nb–0.1Mo	0.59	0.54	0.57	0.58
Zr–1Nb–0.3Mo	0.54	0.49	0.52	0.50
Zr–1Nb–0.5Mo	0.54	0.51	0.50	0.42
Zr–1Nb–0.7Mo	0.46	0.51	0.43	0.46
	f_n (as cold-rolled)	f_n (annealed at 600°C)		
		1 h	4 h	8 h
Zr–1Nb–0.5Sn–0.1Fe	0.56	0.56	0.55	0.56
Zr–1Nb–0.5Sn–0.5Mo–0.1Fe	0.52	0.56	0.55	0.54
Zr–1Nb–0.5Sn–0.2Mo–0.1Fe	0.44	0.50	0.47	0.47
Zr–1Nb–0.5Sn–0.7Mo–0.1Fe	0.45	0.47	0.48	0.52
Zr–1Nb–0.7Sn–0.1Fe	0.49	0.51	0.53	0.49
Zr–1Nb–0.7Sn–0.2Mo–0.1Fe	0.51	0.59	0.56	0.56
Zr–1Nb–0.7Sn–0.5Mo–0.1Fe	0.45	0.52	0.49	0.48
Zr–1Nb–1Sn–0.7Mo–0.1Fe	0.48	0.50	0.49	0.50
Zr–1Nb–1Sn–0.1Fe	0.55	0.58	0.57	0.58
Zr–1Nb–1Sn–0.2Mo–0.1Fe	0.51	0.55	0.55	0.54
Zr–1Nb–1Sn–0.5Mo–0.1Fe	0.48	0.50	0.51	0.51
Zr–1Nb–1Sn–0.7Mo–0.1Fe	0.47	0.52	0.50	0.48

f_n: Kearns number for the surface normal direction.

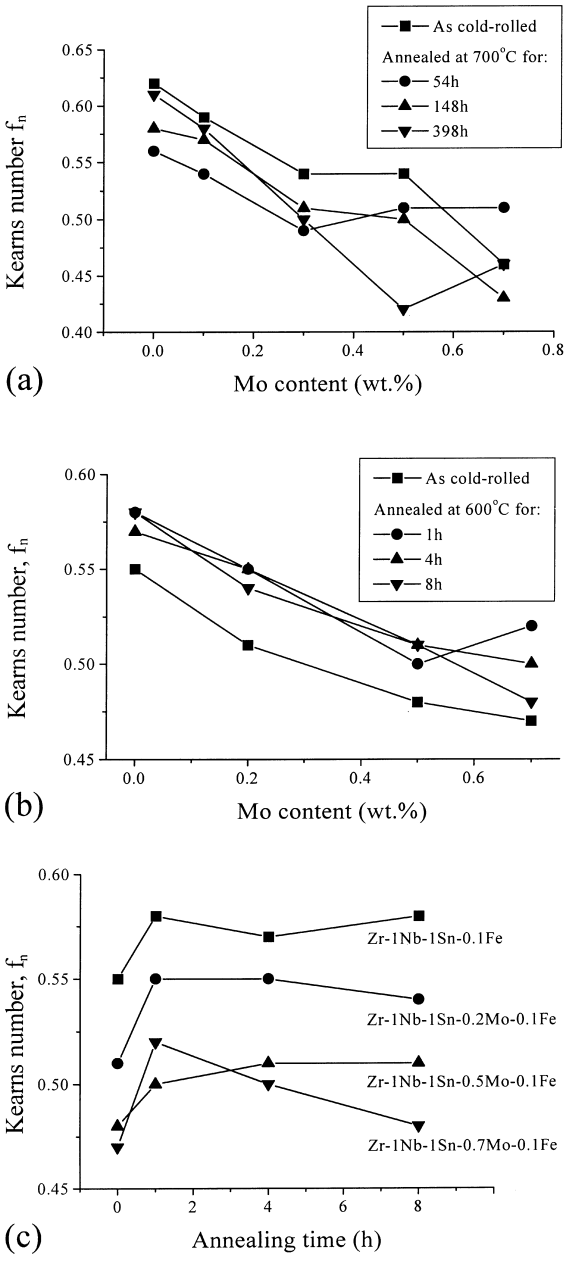

Fig. 8. Variation of the surface normal texture (Kearns no., f_n) as a function of Mo of (a) Zr–1Nb–xMo alloys, (b) Zr–1Nb–1Sn–xMo–0.1Fe alloys, and (c) as a function of heat treating time at 600°C of Zr–1Nb–1Sn–xMo–0.1Fe alloys.

mental for irradiation growth and creep resistance [31,32]. Mo addition in Zr-based alloys results in solid solution hardening, increased rate of work hardening due to lowered stacking fault energy [15] or possible precipitation hardening. Therefore it can be used to substitute work hardening, which can lead to reducing unnecessary cold working.

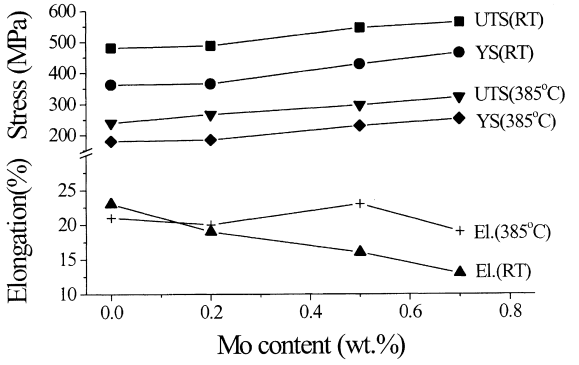

Fig. 9. Effect of Mo on the tensile properties of Zr–1Nb–1Sn–xMo–0.1Fe alloys annealed at 600°C for 8 h.

The strengthening role of Mo may be particularly useful at high temperature. During steady state creep deformation, for example, the rate of dislocation generation is balanced by dynamic recovery. As is known in some high temperature alloys [33–35], Mo is expected to enhance the creep resistance in Zr-base alloys. It is conjectured that increased creep resistance will be realized probably because of the effect of Mo in decreasing the rate of dynamic recovery of recrystallization. Since generation and annihilation of dislocations govern the steady state creep, this implies a sluggish diffusion in Mo-containing alloys. The most probable cause of the retarded diffusion is perhaps the solute dragging effect of Mo, which also contributed in restraining grain coarsening in the Zr–1Nb–xMo alloys as described above. Another possibility is clustering of Mo atoms that may stabilize dislocation substructure efficiently. In fact, 'anneal hardening' was observed by Jonas et al. [36] in Zr–(2.5–20)wt% Nb alloys, which was attributed to clustering of Nb atoms. A similar phenomenon may occur for Mo atoms also, and furthermore, an interactive bonding between Mo and Nb may also occur and increase the stability of clusters.

4. Conclusions

The present study suggests that Mo be wisely utilized as an important alloying element in designing Zr-base alloys. Mo addition suppresses general grain coarsening as well as abnormal growth during extended exposure at high temperature, which is important in materials processing. Relaxation of the normal basal textures by Mo addition may be an attractive merit for pressure tube application. Solid solution hardening effect of Mo can substitute work hardening so that the excessive amount of plastic work for the purpose of strengthening can be avoided. At a proper amount of Mo content, therefore, adequate strengthening can be achieved with minimal

Table 5
Tensile properties of experimental Zr–1Nb–*y*Sn–*x*Mo–0.1Fe alloys annealed at 600°C for 8 h

Alloy	Room temperature			385°C		
	UTS (MPa)	YS (MPa)	El. (%)	UTS (MPa)	YS (MPa)	El. (%)
Zr–1Nb–0.5Sn–0.1Fe	413	330	26	–	–	–
Zr–1Nb–0.5Sn–0.2Mo–0.1Fe	522	397	16	272	206	19
Zr–1Nb–0.5Sn–0.5Mo–0.1Fe	536	404	15	286	224	17
Zr–1Nb–0.5Sn–0.7Mo–0.1Fe	573	453	11	339	271	17
Zr–1Nb–0.7Sn–0.1Fe	440	339	21	227	194	18
Zr–1Nb–0.7Sn–0.2Mo–0.1Fe	481	367	20	259	194	21
Zr–1Nb–0.7Sn–0.5Mo–0.1Fe	516	417	14	287	207	20
Zr–1Nb–0.7Sn–0.7Mo–0.1Fe	550	446	16	337	272	19
Zr–1Nb–1Sn–0.1Fe	481	363	23	240	180	21
Zr–1Nb–1Sn–0.2Mo–0.1Fe	488	366	19	267	185	20
Zr–1Nb–1Sn–0.5Mo–0.1Fe	546	429	16	297	230	23
Zr–1Nb–1Sn–0.7Mo–0.1Fe	563	464	13	321	252	19
Zr–2.5Nb (Recrystallized) [a]	448	310	20	–	–	–

[a] ASTM B 352

sacrifice of ductility and the favorable combination of the mechanical properties is expected to yield a better creep resistance also.

Acknowledgements

This work was supported by the Korea Atomic Energy Research Institute through the Korean Ministry of Science and Technology long-range basic research program for atomic energy.

References

[1] Anon, Fuel design: high burnup offers attractive possibilities, Nuclear Engineering International (Incorporates Nuclear Power) 35(428) (1990).
[2] P.M. Lang, Further burnup extension-Results of IAEA's WREBUS study, Annual Meeting of the American Nuclear Society (ANS), Transactions of the American Nuclear Society, vol. 63, 1991.
[3] R.J. Comstock, G. Schoenberger, G.P. Sabol, ASTM STP 1295 (1996) 710.
[4] A.V. Nikulina, V.A. Markelov, M.M. Peregud, Y.K. Bibilashvili, V.A. Kotrekhov, A.F. Lositsky, N.V. Kuzmenko, U.P. Shevnin, V.K. Shamardin, G.P. Kobylyansky, A.E. Novoselov, ASTM STP 1295 (1996) 785.
[5] B.A. Cheadle, R.A. Holt, V. Fidleris, A.R. Causey, V.F. Urbanic, ASTM STP 754 (1982) 193.
[6] C.D. Wiliams, C.E. Ells, P.R. Dixon, Can. Metall. Quart. 11 (1972) 257.
[7] G.J.C. Carpenter, J.F. Walters, ASTM STP 551 (1974) 400.
[8] J.H. Kim, S.K. Hwang, M.H. Kim, S.I. Kwun, Y.S. Kim, J. Kor. Inst. Met. Mater. 35 (1997) 1271.
[9] J.J. Kearns, Thermal Expansion and Preferred Orientation in Zircaloy, Westinghouse Elec. Co. Report, WAPD TM-472, 1965.
[10] C.P. Gazarra, AMMRC TR-75-4, 1975.
[11] R.G. Fleck, E.G. Price, B.A. Cheadle, ASTM STP 824 (1984) 88.
[12] P. Cotterill, P.R. Mould, Recrystallization and Grain Growth in Metals, Wiley, New York, 1976.
[13] F.J. Humphreys, M. Hartherly, Recrystallization and Related Annealing Phenomena, Pergamon, New York, 1996.
[14] S.G. Oh, S.K. Hwang, J.I. Lee, J. Kor. Inst. Met. Mater. 30 (1992) 929.
[15] B. Heritier, J.J. Jonas, Metall. Trans. 10A (1979) 557.
[16] A. Rogerson, J. Nucl. Mater. 159 (1988) 43.
[17] B.A. Cheadle, R.A. Holt, V. Fidleris, A.R. Causey, V.F. Urbanic, ASTM STP 754 (1982) 193.
[18] E. Tenckhoff, Metall. Trans. 9A (1978) 1401.
[19] E. Tenckhoff, STP 754 (1982) 5.
[20] R.G. Ballinger, G.E. Lucas, R.M. Pelloux, J. Nucl. Mater. 126 (1984) 53.
[21] A.V. Chirkin, A.S. Al-Nakow, J. Nucl. Mater. 183 (1991) 62.
[22] J. Crepin, T. Bretheau, D. Caldemaison, Acta Metall. Mater. 43 (1995) 3709.
[23] R.A. Holt, S.A. Aldridge, J. Nucl. Mater. 135 (1985) 246.
[24] Salinas-Rodriguez, Acta Metall. Mater. 43 (1995) 485.
[25] B.A. Cheadle, C.E. Ells, Electrochem. Technol. 4 (1966) 329.
[26] S.K. Hwang, H.S. Ryoo, J.W. Morris Jr., Metall. Trans. A 22A (1991) 2247.
[27] F. Povolo, J.D. Hermida, A.J. Marzocca, J. Nucl. Mater. 125 (1984) 249.
[28] D.B. Knorr, R.M. Pelloux, Metall. Trans. 13A (1982) 73.
[29] A. Tasooji, R.E. Einziger, A.K. Miller, ASTM STP 824 (1984) 595.

[30] B.A. Cheadle, C.E. Ells, W. Evans, J. Nucl. Mater. 23 (1967) 199.
[31] R.B. Adamson, ASTM STP 633 (1977) 326.
[32] R.A. Holt, J. Nucl. Mater. 59 (1976) 234.
[33] D. Banerjee, A.K. Gogia, T.K. Nandy, K. Muraleedharan, R.S. Mishra, Proceedings of the First International Symposium on Structural Intermetallics, Pennsylvania, USA, September 26–30, The Minerals, Metals and Materials Society, Pennsylvania, 1993.
[34] T.L. Lin, Y. Zhang, Proceedings of the First International Symposium on Structural Intermetallics, Pennsylvania, USA, September 26–30, The Minerals, Metals and Materials Society, Pennsylvania, 1993.
[35] T. Maeda, M. Okada, Y. Shida, Mater. Res. Soc. Proc. 213 (1991) 555.
[36] J.J. Jonas, B. Heritier, M.J. Luton, Metall. Trans. 10A (1979) 611.